*actuators*

MDPI

*Article*

# Steady-State Disturbance-Rejection Controllability for LTI Systems with Rigid-Body Mode

**Haemin Lee [1] and Jinseong Park [2,*]**

[1] Department of Mechanical and Automotive Engineering, Kongju National University, Cheonan 31080, Republic of Korea; leehm@kongju.ac.kr
[2] Department of Mechatronics Engineering, Chungnam National University, Daejeon 34134, Republic of Korea
* Correspondence: js.park@cnu.ac.kr

**Abstract**

Controllability metrics based on system Gramians have been widely adopted to provide quantitative measures of the degree of controllability (DoC) and the disturbance rejection capability (DoDR) of dynamical systems. While steady-state Gramian formulations offer closed-form tractability, they are not applicable when rigid-body modes are present, as the associated poles at the origin cause the conventional Gramians to diverge. This paper presents a novel steady-state DoDR metric for linear time-invariant systems with a rigid-body mode. By block-diagonalizing the dynamics through a similarity transformation and analyzing the asymptotic behavior of the Gramian matrices, we derive an exact closed-form expression for the steady-state DoDR. The resulting formulation is numerically stable and enables systematic evaluation of disturbance-rejection capability even in the presence of a rigid-body mode. The proposed metric is validated using a mass–spring–damper chain model, where its effectiveness is demonstrated in actuator placement problems. The results show that the metric not only remains computationally well-posed but also provides physically meaningful interpretations consistent with modal characteristics. This study establishes a foundation for extending disturbance-rejection metrics to systems with multiple rigid-body modes, thereby broadening the applicability of Gramian-based controllability analysis.

**Keywords:** degree of controllability (DoC); degree of disturbance rejection (DoDR); rigid-body mode; steady-state solution; Gramian matrices; actuator placement

check for updates

Academic Editors: Seenith Sivasundaram, Thomas Yang and Yan Wu

Received: 26 September 2025
Revised: 7 November 2025
Accepted: 11 November 2025
Published: 3 December 2025

**Citation:** Lee, H.; Park, J. Steady-State Disturbance-Rejection Controllability for LTI Systems with Rigid-Body Mode. *Actuators* **2025**, *14*, 589. https://doi.org/10.3390/act14120589

**Copyright:** © 2025 by the authors. Licensee MDPI, Basel, Switzerland. This article is an open access article distributed under the terms and conditions of the Creative Commons Attribution (CC BY) license (https://creativecommons.org/licenses/by/4.0/).

## 1. Introduction

Controllability is a fundamental property of dynamical systems and is often regarded as a prerequisite for proper system operation. Classical tests such as the controllability matrix rank condition, the positive definiteness of the controllability Gramian, and the Popov–Belevitch–Hautus (PBH) test are widely used, but they provide only binary information and can be highly sensitive to parameter perturbations in certain conditions [1]. To overcome these limitations, numerous metrics have been proposed to quantify the degree of controllability (DoC), including controllability norms [2], extended PBH tests [3], modal controllability measures [4], and energy-based characterizations using the minimum 2-norm of uncontrollable initial conditions [5]. Among these, Gramian-based DoC metrics have become the most prevalent due to their closed-form tractability and direct physical interpretation. Building on the observation that the minimum control energy is intrinsically linked to the controllability Gramian [6], these metrics have been widely employed and

extended beyond standard LTI systems to descriptor systems [7,8], nonlinear systems [9,10], bilinear systems [11,12], and network systems [13,14].

One of the most important applications of Gramian-based DoC metrics is optimal actuator placement [15–18]. However, conventional DoC measures do not directly address the system's ability to reject external disturbances, which is often critical in actuator allocation. In practical control systems, external disturbances and cyber–physical uncertainties are inevitable, and numerous controller- and observer-based strategies have been developed to mitigate their effects [19,20]. These studies, however, focus on controller synthesis after the actuator configuration has been fixed. In contrast, it is also important to evaluate the inherent disturbance-rejection capability of a system structure itself, independent of any particular controller design, which motivates the development of the disturbance-rejection controllability metric. Early approaches attempted to maximize disturbance rejection using frequency–domain transfer function methods [21,22], but these are limited when disturbances span arbitrary frequency ranges. In addition, frequency–domain formulations are inherently restricted to steady-state sinusoidal inputs and rely on spectral representations that do not directly capture broadband disturbances commonly encountered in mechanical systems. Moreover, transfer-function-based formulations are fundamentally limited in extending to multi-input–multi-output (MIMO) systems, since disturbance-rejection characteristics cannot be represented by a single frequency response and depend on the choice of input–output pairs and weighting functions. In contrast, Gramian-based time-domain methods provide a unified and coordinate-invariant framework that naturally accommodates MIMO dynamics. Consequently, the focus of subsequent research has shifted toward time–domain formulations that quantify disturbance rejection through system Gramians, enabling a more general and quantitative characterization of disturbance responses. Mirza and Van Niekerk [23] proposed a disturbance sensitivity Gramian in the time domain, though its dependence on the feedback gain restricted its applicability. A key advance was made by Kang et al. [24], who introduced the degree of disturbance rejection (DoDR) metric for open-loop systems, formulated via controllability and disturbance Gramians, and later extended in related studies [25,26]. Building on this foundation, Xia et al. [27] combined DoC and DoDR into a unified Gramian-based framework and applied it to wind turbine systems [28,29], while Jeong and Park [30] extended DoDR concepts to active noise control.

Despite their closed-form tractability, Gramian-based metrics typically require solving differential equations and remain dependent on the final time horizon, motivating the use of algebraic steady-state solutions available only for asymptotically stable systems. For unstable dynamics, prior studies [17,31] separated stable and anti-stable contributions, which prevented simultaneous energy characterization. This limitation was resolved by Lee and Park [32], who derived a unified steady-state DoC metric that accounts for both stable and unstable subsystems, demonstrating that the total control energy equals the sum of subsystem contributions and enabling efficient computation for unstable systems. Building on this framework, subsequent work extended the concept to disturbance-rejection analysis, deriving a steady-state solution of the DoDR metric for unstable systems and thereby enabling a quantitative assessment of disturbance-rejection capability in the presence of unstable modes [33].

While the aforementioned studies provide meaningful metrics for unstable systems, their applicability is limited to cases where system poles lie strictly in the left- and right-half planes. In particular, these formulations break down when poles are located on the imaginary axis, as in the presence of undamped modes. To address this issue, various approaches have been investigated [34–37], most of which introduce small perturbations in the form of artificial light damping to ensure stability of the Gramian-based solutions. However, such methods inherently depend on the structure and magnitude of the artificially

added damping, leading to results that lack robustness. More recently, Lee [38] resolved this limitation by defining the Gramians in the Laplace domain and employing the generalized final value theorem, thereby deriving an exact steady-state DoDR metric without the need for small perturbations. This metric yields accurate disturbance-rejection solutions for undamped flexible structures with nonzero natural frequencies. Nevertheless, it does not account for rigid-body motions, where the natural frequency vanishes and poles reside at the origin. Consequently, the problem of evaluating disturbance-rejection capability in systems with rigid-body modes remains open.

Motivated by these challenges, the present study develops a steady-state formulation of the DoDR metric that remains valid even when a rigid-body mode is present, representing a system with a single zero eigenvalue commonly found in mechanical structures. While previous results have successfully addressed unstable or oscillatory modes, the case of rigid-body dynamics where poles lie at the origin has remained unresolved. The primary novelty of this work lies in the analytical treatment, providing the first closed-form steady-state solution for the DoDR metric in systems that contain a single zero eigenvalue, a case not covered by previous formulations restricted to asymptotically stable systems. The blockwise decomposition and Schur complement framework are employed as analytical tools to systematically characterize the influence of the zero-eigenvalue mode within the overall Gramian structure. The single rigid-body case analyzed in this study represents an initial step toward extending the proposed framework to systems with multiple rigid-body modes, such as flexible multibody structures or large-scale mechanical networks, which will be addressed in future work.

The remainder of this paper is organized as follows. Section 2 reviews the conventional formulation of the DoDR metric and its steady-state expression for asymptotically stable systems. Section 3 extends the analysis to systems that include a single rigid-body mode, deriving the closed-form steady-state disturbance-rejection metric through a blockwise Gramian decomposition. Section 4 presents numerical examples based on mass–spring–damper chains, illustrating both the numerical robustness of the proposed formulation and its implications for actuator placement. Finally, Section 5 concludes the paper and discusses directions for future research, including extensions to systems with multiple rigid-body modes.

## 2. Preliminaries

This section provides an overview of the DoDR metric originally proposed by Kang et al. [24], together with its standard closed-form expression for asymptotically stable systems. We begin by considering a controllable linear time-invariant (LTI) system described by

$$\dot{x}(t) = Ax(t) + Bu(t) + Dw(t), \tag{1}$$

where $x(t) \in \mathbb{R}^n$ denotes the state vector, $u(t) \in \mathbb{R}^r$ the control input, and $w(t) \in \mathbb{R}^p$ the disturbance. The system matrices $A$, $B$, and $D$ are assumed to be constant and of appropriate dimensions.

In practical systems, external disturbances acting on mechanical or control systems generally contain multiple frequency components and may be band-limited rather than perfectly white. However, any such band-limited disturbance can be equivalently represented as the output of an appropriate shaping filter driven by a signal with flat power spectral density. If necessary, this shaping filter can be incorporated into the system dynamics by augmenting the state-space matrices $A$ and $D$. Therefore, without loss of generality, the disturbance $w(t)$ is modeled as a zero-mean Gaussian white noise (GWN) process with correlation function

$$R_w(\tau) = \mathbb{E}\left[w(t)w^\top(t+\tau)\right] = S_w\delta(\tau), \tag{2}$$

where $S_w \succ 0$ denotes the disturbance covariance. This disturbance modeling approach is consistent with that adopted in the original work, where the concept of the DoDR was first introduced.

The disturbance-rejection controllability metric, referred to as DoDR, is then defined as the minimal control energy required to drive the system from the zero state back to the origin in the presence of the disturbance:

$$\rho(t) := \min_u \mathbb{E}\left[\int_0^t u^\top(\tau)u(\tau)d\tau\right], \tag{3}$$

subject to $x(0) = 0$, $x(t) = 0$, and the dynamics in (1). A smaller value of $\rho(t)$ indicates that less control effort is needed to suppress the disturbance and, hence, the system exhibits superior disturbance-rejection capability.

It is well known that (3) admits the closed-form solution as given in Kang et al. [24]

$$\rho(t) = \mathrm{tr}\Big(W^{-1}(t)\Sigma(t)\Big), \tag{4}$$

where the matrices

$$W(t) = \int_0^t e^{A\tau}BB^\top e^{A^\top\tau}d\tau, \tag{5}$$

$$\Sigma(t) = \int_0^t e^{A\tau}DS_wD^\top e^{A^\top\tau}d\tau \tag{6}$$

are referred to as the *controllability Gramian* and the *disturbance Gramian*, respectively.

The matrix $W(t)$ is positive definite for any $t > 0$ under the controllability assumption, ensuring that the inverse in (4) is well defined. The two Gramians in (5) and (6) satisfy the differential Lyapunov equations:

$$\dot{W}(t) = AW(t) + W(t)A^\top + BB^\top, \tag{7}$$

$$\dot{\Sigma}(t) = A\Sigma(t) + \Sigma(t)A^\top + DS_wD^\top, \tag{8}$$

whose solutions directly yield the quantities in (4).

Although the DoDR provides a meaningful quantitative measure for assessing the disturbance-rejection capability of a system, its computation generally requires solving the differential equations in (7) and (8), which can be computationally demanding. In addition, the DoDR expression in (4) depends explicitly on the final time $t$, so its value may vary with the chosen time horizon, making it difficult to obtain a representative performance index for the system. To address both the computational cost and the time-dependence issue, it is common to replace the time-varying formulation (4) with its steady-state counterpart whenever possible.

The Gramians defined in (5) and (6) admit steady-state limits if the system is asymptotically stable, i.e., when $A$ is a Hurwitz matrix. In that case, the steady-state Gramians $\bar{W}$ and $\bar{\Sigma}$ satisfy the algebraic Lyapunov equations:

$$A\bar{W} + \bar{W}A^\top + BB^\top = 0, \tag{9}$$

$$A\bar{\Sigma} + \bar{\Sigma}A^\top + DS_wD^\top = 0, \tag{10}$$

and the steady-state disturbance-rejection metric is then given by

$$\bar{\rho} = \mathrm{tr}\Big(\bar{W}^{-1}\bar{\Sigma}\Big). \tag{11}$$

Since the algebraic Equations (9) and (10) can be solved directly without integrating the differential Equations (7) and (8), the steady-state Formula (11) avoids the computational burden associated with the original definition (4). Furthermore, it eliminates the explicit dependence on $t$, yielding a time-invariant performance index.

It is important to note, however, that the steady-state Gramians in (9) and (10) exist only when all eigenvalues of $A$ lie in the open left-half complex plane. If $A$ has eigenvalues at the origin, i.e., the system possesses zero eigenvalue modes such as rigid-body motions, both $W(t)$ and $\Sigma(t)$ grow unboundedly as $t \to \infty$. Consequently, the steady-state expression (11) is not applicable when zero eigenvalues are present, and the effect of these modes on the disturbance-rejection metric remains unclear. Motivated by this limitation, the next section develops an alternative formulation of the DoDR that explicitly addresses the case where $A$ has a single zero eigenvalue mode in addition to asymptotically stable modes. This constitutes the scope of the present paper. Focusing on this simplest scenario allows us to rigorously characterize the Gramian behavior in the presence of a zero eigenvalue, while also laying the foundation for future extensions to cases involving multiple zero eigenvalues.

## 3. DoDR Formulation for Systems with a Single Zero Eigenvalue

The previous section has shown that the steady-state disturbance-rejection metric admits a closed-form expression when all eigenvalues of the system matrix $A$ lie strictly in the open left-half complex plane. However, when $A$ possesses a single zero eigenvalue, corresponding to a rigid-body mode, the controllability and disturbance Gramians diverge as the time horizon grows, rendering the standard steady-state formula inapplicable. This section develops a formulation of the disturbance-rejection metric that explicitly addresses systems comprising both asymptotically stable modes and a single zero eigenvalue mode. We first represent the Gramians in a blockwise structure according to the spectral decomposition of $A$, analyze the growth rates of the individual blocks, and show that all cross terms vanish as the time horizon tends to infinity. By introducing a suitable normalization for the zero-eigenvalue block, we then derive a closed-form steady-state expression that characterizes the disturbance-rejection metric in the presence of a single zero eigenvalue.

### *3.1. Problem Setup and Blockwise Representation*

Consider a linear time-invariant system in which the system matrix $A$ contains both asymptotically stable eigenvalues and a single zero eigenvalue, the latter typically associated with a rigid-body mode. Since the previous section confirmed that the steady-state solution of the DoDR metric exists when $A$ is Hurwitz, this motivates extending the analysis to the case where $A$ includes both stable and zero eigenvalue modes. To this end, the system matrix $A$ is decomposed into two blocks, one corresponding to the stable eigenvalues and the other to the single zero eigenvalue. In general, such a block decomposition can be achieved through a similarity transformation [39]; therefore, without loss of generality, $A$ can be represented by a linear transformation of the state vector $x$ in the block-diagonal form that separates these two types of modes. For simplicity, this paper adopts the following block-diagonal representation of $A$ without explicitly describing the transformation process. Specifically, let

$$A = \begin{bmatrix} A_s & 0 \\ 0 & A_0 \end{bmatrix}, \tag{12}$$

where $A_s \in \mathbb{R}^{(n-1)\times(n-1)}$ is Hurwitz with $\mathrm{Re}(\lambda(A_s)) < 0$, and $A_0 = 0 \in \mathbb{R}$ represents the single zero eigenvalue mode. The state, control, and disturbance matrices are partitioned accordingly as

$$B = \begin{bmatrix} B_s \\ B_0 \end{bmatrix}, \qquad D = \begin{bmatrix} D_s \\ D_0 \end{bmatrix}, \tag{13}$$

so that the system dynamics can be written in the decoupled form

$$\begin{bmatrix} \dot{x}_s(t) \\ \dot{x}_0(t) \end{bmatrix} = \begin{bmatrix} A_s & 0 \\ 0 & A_0 \end{bmatrix} \begin{bmatrix} x_s(t) \\ x_0(t) \end{bmatrix} + \begin{bmatrix} B_s \\ B_0 \end{bmatrix} u(t) + \begin{bmatrix} D_s \\ D_0 \end{bmatrix} w(t). \tag{14}$$

Since we assumed that $(A, B)$ is controllable, $(A_s, B_s)$ is controllable, and in the single zero eigenvalue case this further implies that $B_0 \neq 0$ so that $(A_0, B_0)$ is controllable. This blockwise representation enables us to analyze the controllability and disturbance Gramians on each subspace separately, laying the foundation for deriving a closed-form steady-state disturbance-rejection metric that accounts for both asymptotically stable modes and a single zero eigenvalue mode.

Having introduced the block-diagonal representation (12)–(14), we next express the controllability and disturbance Gramians in the same blockwise form. From the definition of the controllability and disturbance Gramians in (5)–(6), both Gramians naturally admit a block structure:

$$W(t) = \begin{bmatrix} W_{ss}(t) & W_{s0}(t) \\ W_{0s}(t) & W_{00}(t) \end{bmatrix}, \qquad \Sigma(t) = \begin{bmatrix} \Sigma_{ss}(t) & \Sigma_{s0}(t) \\ \Sigma_{0s}(t) & \Sigma_{00}(t) \end{bmatrix}, \tag{15}$$

where each block is defined as

$$W_{ij}(t) = \int_0^t e^{A_i\tau} B_i B_j^\top e^{A_j^\top \tau} d\tau, \qquad \Sigma_{ij}(t) = \int_0^t e^{A_i\tau} D_i S_w D_j^\top e^{A_j^\top \tau} d\tau, \tag{16}$$

for $i, j \in \{s, 0\}$, with the subsystem matrices $A_s$, $A_0$, $B_s$, $B_0$, $D_s$, and $D_0$ as defined in (12) and (13). The block matrices satisfy the following properties.

**Lemma 1** (Convergence of stable-block Gramians)**.** *The block matrices*

$$W_{ss}(t) = \int_0^t e^{A_s\tau} B_s B_s^\top e^{A_s^\top \tau} d\tau, \qquad \Sigma_{ss}(t) = \int_0^t e^{A_s\tau} D_s S_w D_s^\top e^{A_s^\top \tau} d\tau \tag{17}$$

*converge as $t \to \infty$ to the unique solutions $\bar{W}_{ss}$ and $\bar{\Sigma}_{ss}$ of the algebraic Lyapunov equations*

$$A_s \bar{W}_{ss} + \bar{W}_{ss} A_s^\top + B_s B_s^\top = 0, \qquad A_s \bar{\Sigma}_{ss} + \bar{\Sigma}_{ss} A_s^\top + D_s S_w D_s^\top = 0. \tag{18}$$

**Proof.** Since $A_s$ is Hurwitz, $e^{A_s\tau}$ exponentially decays to zero, and the integrals defining $W_{ss}(t)$ and $\Sigma_{ss}(t)$ converge as $t \to \infty$. Differentiating $W_{ss}(t)$ with respect to time gives

$$\dot{W}_{ss}(t) = A_s W_{ss}(t) + W_{ss}(t) A_s^\top + B_s B_s^\top, \tag{19}$$

whose steady-state solution satisfies the first equation in (18). An identical argument applies to $\Sigma_{ss}(t)$. Hence the limits $\bar{W}_{ss}$ and $\bar{\Sigma}_{ss}$ exist and are unique. See also [24,39]. □

**Lemma 2** (Growth of the zero-eigenvalue block)**.** *Suppose $A_0 = 0 \in \mathbb{R}$ represents the single zero eigenvalue mode. Then, for all $t \geq 0$, the block matrices simplify to*

$$W_{00}(t) = t B_0 B_0^\top, \qquad \Sigma_{00}(t) = t D_0 S_w D_0^\top. \tag{20}$$

**Proof.** Since $A_0 = 0$, the matrix exponential satisfies

$$e^{A_0 \tau} = 1. \tag{21}$$

Substituting into the definitions of $W_{00}(t)$ and $\Sigma_{00}(t)$ gives

$$W_{00}(t) = \int_0^t B_0 B_0^\top d\tau = t B_0 B_0^\top, \qquad \Sigma_{00}(t) = \int_0^t D_0 S_w D_0^\top d\tau = t D_0 S_w D_0^\top, \tag{22}$$

which completes the proof. □

**Remark 1.** *As shown in Lemma 2, the zero-eigenvalue blocks $W_{00}(t)$ and $\Sigma_{00}(t)$ grow linearly with t according to (20). Since both terms diverge as $t \to \infty$, the overall controllability Gramian $W(t)$ and disturbance Gramian $\Sigma(t)$ also diverge, which explains why the classical steady-state disturbance-rejection metric cannot be directly applied when a zero eigenvalue mode is present.*

**Lemma 3** (Closed-form limits of off-diagonal blocks)**.** *Under $A_0 = 0 \in \mathbb{R}$ and $A_s$ Hurwitz, the off-diagonal blocks in (15) converge as $t \to \infty$ and admit the closed-form limits:*

$$\bar{W}_{s0} = -A_s^{-1} B_s B_0^\top, \qquad \bar{W}_{0s} = -B_0 B_s^\top (A_s^\top)^{-1}, \tag{23}$$

$$\bar{\Sigma}_{s0} = -A_s^{-1} D_s S_w D_0^\top, \qquad \bar{\Sigma}_{0s} = -D_0 S_w D_s^\top (A_s^\top)^{-1}. \tag{24}$$

**Proof.** Consider $W_{s0}(t) = \int_0^t e^{A_s \tau} B_s B_0^\top e^{A_0^\top \tau} d\tau$. Since $A_0 = 0$, $e^{A_0^\top \tau} = 1$. Moreover, $A_s$ is Hurwitz, so

$$\int_0^\infty e^{A_s \tau} d\tau = -A_s^{-1}. \tag{25}$$

Hence,

$$\bar{W}_{s0} = \int_0^\infty e^{A_s \tau} B_s B_0^\top d\tau = \Big( \int_0^\infty e^{A_s \tau} d\tau \Big) B_s B_0^\top = -A_s^{-1} B_s B_0^\top. \tag{26}$$

The other blocks follow analogously. Since $W_{0s}(t) = W_{s0}^\top(t)$ and $\Sigma_{0s}(t) = \Sigma_{s0}^\top(t)$, their steady-state limits directly yield $\bar{W}_{0s} = \bar{W}_{s0}^\top$ and $\bar{\Sigma}_{0s} = \bar{\Sigma}_{s0}^\top$. □

The preceding lemmas have established the convergence properties of all relevant Gramian blocks: the stable–stable blocks converge to finite steady-state limits, the zero–zero blocks grow linearly with time, and the off-diagonal blocks admit closed-form steady-state limits. Together, these results provide a complete blockwise characterization of the controllability and disturbance Gramians for systems with both asymptotically stable modes and a single zero eigenvalue mode. In the next subsection, we exploit these properties to show that all cross terms vanish as $t \to \infty$, thereby enabling a closed-form disturbance-rejection metric that incorporates the effect of a single zero eigenvalue mode into the classical formulation.

### *3.2. Vanishing Cross Terms in the DoDR Expansion*

To investigate the asymptotic behavior of the disturbance-rejection metric, we first express the inverse of the controllability Gramian using the blockwise inversion formula based on the Schur complement. Given the block representation of the controllability Gramian in (15), the inverse $W^{-1}(t)$ admits the standard block representation shown below. This formulation enables us to separate the contributions of the stable modes, the single zero-eigenvalue mode, and the associated cross terms in the DoDR metric. The inversion follows the standard blockwise inversion formula based on the Schur complement [40]:

$$\begin{bmatrix} A & B \\ C & D \end{bmatrix}^{-1} = \begin{bmatrix} A^{-1} + A^{-1}BS^{-1}CA^{-1} & -A^{-1}BS^{-1} \\ -S^{-1}CA^{-1} & S^{-1} \end{bmatrix}, \qquad S = D - CA^{-1}B. \tag{27}$$

Applying this formula to the controllability Gramian in (15) yields

$$W^{-1}(t) = \begin{bmatrix} W_{ss}^{-1}(t) + W_{ss}^{-1}(t)W_{s0}(t)W_{0s}(t)W_{ss}^{-1}(t)/s_{00}(t) & -W_{ss}^{-1}(t)W_{s0}(t)/s_{00}(t) \\ -W_{0s}(t)W_{ss}^{-1}(t)/s_{00}(t) & 1/s_{00}(t) \end{bmatrix}, \tag{28}$$

where the Schur complement $s_{00}(t) \in \mathbb{R}$ is given by

$$s_{00}(t) = W_{00}(t) - W_{0s}(t)W_{ss}^{-1}(t)W_{s0}(t). \tag{29}$$

Since the system contains a single zero eigenvalue mode, the $(2,2)$ block of the controllability Gramian is scalar. Accordingly, the Schur complement $s_{00}(t) \in \mathbb{R}$ represents the scalar adjustment term arising from this blockwise inversion. In addition, since $W(t) \succ 0$ and $W_{ss}(t) \succ 0$ for any $t > 0$ under controllability, the scalar $s_{00}(t)$ is strictly positive. Therefore, its reciprocal $1/s_{00}(t)$ is well-defined. Substituting (28) into the finite-horizon DoDR expression (4) and using the blockwise disturbance Gramian in (15), we expand the trace as follows:

$$\rho(t) = \rho_{ss}(t) + \rho_{00}(t) + \rho_1(t) + \rho_2(t) + \rho_3(t) \tag{30}$$

where

$$\begin{aligned} \rho_{ss}(t) &= \operatorname{tr}\big(W_{ss}^{-1}(t)\Sigma_{ss}(t)\big), \\ \rho_{00}(t) &= \Sigma_{00}(t)/s_{00}(t), \\ \rho_1(t) &= \operatorname{tr}\big(W_{ss}^{-1}(t)W_{s0}(t)W_{0s}(t)W_{ss}^{-1}(t)\Sigma_{ss}(t)\big)/s_{00}(t), \\ \rho_2(t) &= -\operatorname{tr}\big(W_{ss}^{-1}(t)W_{s0}(t)\Sigma_{0s}(t)\big)/s_{00}(t), \\ \rho_3(t) &= -\operatorname{tr}\big(W_{0s}(t)W_{ss}^{-1}(t)\Sigma_{s0}(t)\big)/s_{00}(t). \end{aligned} \tag{31}$$

This blockwise expansion separates the contributions into the stable term $\rho_{ss}(t)$, the single zero-eigenvalue term $\rho_{00}(t)$, and the cross terms $\rho_1(t), \rho_2(t), \rho_3(t)$. In what follows, we show that all cross terms vanish as $t \to \infty$ in the single zero-eigenvalue case, which simplifies the disturbance-rejection metric to the remaining main contributions.

**Lemma 4** (Vanishing of $\rho_1(t)$)**.** *Let*

$$\rho_1(t) = \frac{1}{s_{00}(t)} \operatorname{tr}\Big(W_{ss}^{-1}(t)W_{s0}(t)W_{0s}(t)W_{ss}^{-1}(t)\Sigma_{ss}(t)\Big). \tag{32}$$

*Then*

$$\lim_{t\to\infty} \rho_1(t) = 0. \tag{33}$$

**Proof.** By Lemmas 1 and 3, the factors $W_{ss}^{-1}(t)$, $W_{s0}(t)$, $W_{0s}(t)$, and $\Sigma_{ss}(t)$ converge to finite limits as $t \to \infty$. Hence the scalar

$$N_1(t) := \operatorname{tr}\Big(W_{ss}^{-1}(t)W_{s0}(t)W_{0s}(t)W_{ss}^{-1}(t)\Sigma_{ss}(t)\Big) \tag{34}$$

remains bounded and converges to a finite limit. By Lemma 2, $W_{00}(t) = tB_0B_0^\top$, and therefore

$$s_{00}(t) = W_{00}(t) - W_{0s}(t)W_{ss}^{-1}(t)W_{s0}(t) = tB_0B_0^\top - M(t), \tag{35}$$

where $M(t)$ is bounded because each of $W_{0s}(t)$, $W_{ss}^{-1}(t)$, and $W_{s0}(t)$ converges to a finite matrix. Consequently, $s_{00}(t)$ grows linearly with $t$ since $(A_0, B_0)$ is controllable in the single zero-eigenvalue case, implying $B_0 B_0^\top > 0$. Hence $s_{00}(t) \to \infty$ and $1/s_{00}(t) \to 0$. Combining bounded $N_1(t)$ with $1/s_{00}(t) \to 0$ yields

$$\lim_{t\to\infty} \rho_1(t) = \lim_{t\to\infty} \frac{N_1(t)}{s_{00}(t)} = 0, \tag{36}$$

which proves (33). □

**Corollary 1** (Vanishing of $\rho_2(t)$ and $\rho_3(t)$)**.** *Let*

$$\begin{aligned} \rho_2(t) &= -\frac{1}{s_{00}(t)} \mathrm{tr}\big(W_{ss}^{-1}(t) W_{s0}(t) \Sigma_{0s}(t)\big), \\ \rho_3(t) &= -\frac{1}{s_{00}(t)} \mathrm{tr}\big(W_{0s}(t) W_{ss}^{-1}(t) \Sigma_{s0}(t)\big). \end{aligned} \tag{37}$$

*Then*

$$\lim_{t\to\infty} \rho_2(t) = \lim_{t\to\infty} \rho_3(t) = 0. \tag{38}$$

**Proof.** From Lemmas 1 and 3, the factors $W_{ss}^{-1}(t)$, $W_{s0}(t)$, $W_{0s}(t)$, $\Sigma_{s0}(t)$, and $\Sigma_{0s}(t)$ converge to finite limits as $t \to \infty$. Hence

$$N_2(t) := \mathrm{tr}\big(W_{ss}^{-1}(t) W_{s0}(t) \Sigma_{0s}(t)\big), \qquad N_3(t) := \mathrm{tr}\big(W_{0s}(t) W_{ss}^{-1}(t) \Sigma_{s0}(t)\big) \tag{39}$$

remain bounded and converge to finite limits. Since (35) implies $s_{00}(t) \to \infty$ and therefore $1/s_{00}(t) \to 0$, we obtain

$$\lim_{t\to\infty} \rho_2(t) = -\lim_{t\to\infty} \frac{N_2(t)}{s_{00}(t)} = 0, \qquad \lim_{t\to\infty} \rho_3(t) = -\lim_{t\to\infty} \frac{N_3(t)}{s_{00}(t)} = 0 \tag{40}$$

which proves (38). □

The above results show that all cross terms $\rho_1(t)$, $\rho_2(t)$, and $\rho_3(t)$ vanish in the steady state. Consequently, the steady-state value of the disturbance-rejection metric is entirely determined by the two main contributions, $\rho_{ss}(t)$ and $\rho_{00}(t)$, whose convergence properties and closed-form expressions remain to be analyzed. The next subsection investigates the limits of $\rho_{ss}(t)$ and $\rho_{00}(t)$, thereby establishing the final closed-form expression of the DoDR metric for systems with a single zero eigenvalue mode.

### *3.3. Convergence of the Main Terms and Closed-Form Solution of the DoDR Metric*

Having established that all cross terms vanish in the steady state, we now focus on the two main contributions, $\rho_{ss}(t)$ and $\rho_{00}(t)$, which fully determine the steady-state value of the disturbance-rejection metric. This subsection analyzes the convergence properties of these two terms and, through this analysis, derives their limiting behavior as $t \to \infty$, thereby obtaining closed-form expressions that extend the conventional disturbance-rejection metric to systems with a single zero eigenvalue mode in addition to asymptotically stable modes.

To proceed, we first analyze the individual contributions $\rho_{ss}(t)$ and $\rho_{00}(t)$ in the steady state. The following lemmas establish the convergence of each term and provide the necessary closed-form expressions for the final result.

**Lemma 5** (Convergence of $\rho_{ss}(t)$)**.** *Let*

$$\rho_{ss}(t) = \mathrm{tr}\big(W_{ss}^{-1}(t) \Sigma_{ss}(t)\big). \tag{41}$$

*Then $\rho_{ss}(t)$ converges to a finite limit as $t \to \infty$, given by*

$$\lim_{t\to\infty} \rho_{ss}(t) = \mathrm{tr}\big(\bar{W}_{ss}^{-1}\bar{\Sigma}_{ss}\big), \tag{42}$$

*where $\bar{W}_{ss}$ and $\bar{\Sigma}_{ss}$ are the unique solutions of the Lyapunov equations in (18)*

**Proof.** The convergence of $W_{ss}(t) \to \bar{W}_{ss}$ and $\Sigma_{ss}(t) \to \bar{\Sigma}_{ss}$ was already established in Lemma 1. Since $W_{ss}(t) \succ 0$ for all $t > 0$ under controllability, $\bar{W}_{ss}$ is also positive definite and $\bar{W}_{ss}^{-1}$ is well-defined. Therefore, it follows that $\mathrm{tr}\big(W_{ss}^{-1}(t)\Sigma_{ss}(t)\big)$ converges to $\mathrm{tr}\big(\bar{W}_{ss}^{-1}\bar{\Sigma}_{ss}\big)$ as $t \to \infty$. This proves (42). □

**Lemma 6** (Convergence of $\rho_{00}(t)$)**.** *Let*

$$\rho_{00}(t) = \frac{\Sigma_{00}(t)}{s_{00}(t)}, \tag{43}$$

*where $\Sigma_{00}(t)$ and $s_{00}(t)$ are defined in (20) and (29), respectively. Then $\rho_{00}(t)$ converges to a finite limit as $t \to \infty$, given by*

$$\lim_{t\to\infty} \rho_{00}(t) = \frac{D_0 S_w D_0^\top}{B_0 B_0^\top}. \tag{44}$$

**Proof.** From Lemma 2, the zero-mode blocks of the Gramians satisfy the linear growth relations in (20), namely

$$\Sigma_{00}(t) = t\, D_0 S_w D_0^\top, \qquad W_{00}(t) = t\, B_0 B_0^\top, \tag{45}$$

for all $t \geq 0$. As established in Lemma 4 [see (35)], $s_{00}(t)$ can be written as

$$s_{00}(t) = tB_0B_0^\top - M(t), \tag{46}$$

where $M(t)$ is bounded because each of $W_{0s}(t)$, $W_{ss}^{-1}(t)$, and $W_{s0}(t)$ converges to a finite matrix as $t \to \infty$ (Lemmas 1 and 3). Since $(A_0, B_0)$ is controllable in the single zero-eigenvalue case, we have $B_0 \neq 0$ and thus $B_0B_0^\top > 0$. It follows that $s_{00}(t)$ grows linearly with $t$ and satisfies

$$\lim_{t\to\infty} \frac{s_{00}(t)}{t} = B_0B_0^\top. \tag{47}$$

Combining this with $\Sigma_{00}(t) = t\, D_0 S_w D_0^\top$ gives

$$\rho_{00}(t) = \frac{\Sigma_{00}(t)}{s_{00}(t)} = \frac{t\, D_0 S_w D_0^\top}{s_{00}(t)} = \frac{D_0 S_w D_0^\top}{s_{00}(t)/t}. \tag{48}$$

Taking the limit as $t \to \infty$ yields

$$\lim_{t\to\infty} \rho_{00}(t) = \frac{D_0 S_w D_0^\top}{B_0 B_0^\top}, \tag{49}$$

which proves (44). □

Having established in the preceding lemmas that the cross terms $\rho_1(t)$, $\rho_2(t)$, and $\rho_3(t)$ vanish in the steady state and that the remaining terms $\rho_{ss}(t)$ and $\rho_{00}(t)$ converge to the closed-form expressions (42) and (44), respectively, we are now in a position to combine these results. For the reader's convenience, the following theorem restates all definitions and assumptions used throughout the paper so that the result is entirely self-contained. It then summarizes the steady-state behavior of the disturbance-rejection metric and provides

its closed-form solution for systems with a single zero eigenvalue mode in addition to asymptotically stable modes.

**Theorem 1** (Steady-State Solution of the DoDR Metric)**.** *Consider the linear time-invariant system*

$$\dot{x}(t) = Ax(t) + Bu(t) + Dw(t), \tag{50}$$

*where $x(t) \in \mathbb{R}^n$ is the state, $u(t) \in \mathbb{R}^r$ the control input, and $w(t) \in \mathbb{R}^p$ a zero-mean Gaussian white noise process with covariance $S_w \succeq 0$. The controllability and disturbance Gramians are defined by*

$$W(t) = \int_0^t e^{A\tau} BB^\top e^{A^\top \tau} d\tau, \qquad \Sigma(t) = \int_0^t e^{A\tau} DS_w D^\top e^{A^\top \tau} d\tau. \tag{51}$$

*The finite-horizon disturbance-rejection metric is*

$$\rho(t) = \operatorname{tr}\big(W^{-1}(t)\Sigma(t)\big), \tag{52}$$

*which represents the minimal control energy required to steer the state from $x(0) = 0$ to $x(t) = 0$ over $[0, t]$ in the presence of disturbances. Assume that $(A, B)$ is controllable, so that $W(t) \succ 0$ for any $t > 0$, and that a similarity transformation block-diagonalizes the system as*

$$A = \begin{bmatrix} A_s & 0 \\ 0 & 0 \end{bmatrix}, \qquad B = \begin{bmatrix} B_s \\ B_0 \end{bmatrix}, \qquad D = \begin{bmatrix} D_s \\ D_0 \end{bmatrix}, \tag{53}$$

*where $A_s \in \mathbb{R}^{(n-1)\times(n-1)}$ is Hurwitz. Since $(A, B)$ is controllable, it follows that $(A_s, B_s)$ is controllable and $B_0 \neq 0$, so that the zero eigenvalue mode is also controllable. Define the steady-state metric*

$$\bar{\rho} := \lim_{t\to\infty} \rho(t). \tag{54}$$

*Then $\bar{\rho}$ exists and is given by*

$$\bar{\rho} = \operatorname{tr}\big(\bar{W}_{ss}^{-1}\bar{\Sigma}_{ss}\big) + \frac{D_0 S_w D_0^\top}{B_0 B_0^\top}, \tag{55}$$

*where $\bar{W}_{ss}$ and $\bar{\Sigma}_{ss}$ are the unique solutions of the Lyapunov equations*

$$A_s\bar{W}_{ss} + \bar{W}_{ss}A_s^\top + B_s B_s^\top = 0, \tag{56}$$

$$A_s\bar{\Sigma}_{ss} + \bar{\Sigma}_{ss}A_s^\top + D_s S_w D_s^\top = 0. \tag{57}$$

**Proof.** By Lemma 4 and Corollary 1, the cross terms $\rho_1(t)$, $\rho_2(t)$, and $\rho_3(t)$ vanish as $t \to \infty$. Moreover, Lemmas 5 and 6 give the closed-form limits for $\rho_{ss}(t)$ and $\rho_{00}(t)$. Combining these results with the blockwise expansion of $\rho(t)$ in (30) directly yields (55). □

The closed-form steady-state solution established in Theorem 1 offers several key insights into the disturbance-rejection capability of systems containing both asymptotically stable modes and a single zero eigenvalue mode. First, the derived expression explicitly separates the contributions of the exponentially decaying modes and the linearly growing rigid-body mode, thereby enabling a clear interpretation of how each subsystem influences the overall disturbance-rejection metric. In contrast to the conventional DoDR formulation, which becomes ill-posed in the presence of zero eigenvalues due to the unbounded growth of the Gramians, our result provides a well-defined finite performance index by isolating the dominant linear growth terms and normalizing them appropriately. Consequently, the closed-form solution in (55) resolves the issue of evaluating disturbance-rejection

metrics for systems with rigid-body dynamics, where classical approaches fail to yield meaningful steady-state limits.

In particular, the zero-eigenvalue contribution is given by

$$\bar{\rho}_{00} := \frac{D_0 S_w D_0^\top}{B_0 B_0^\top}, \tag{58}$$

which can be interpreted as a *disturbance-to-control transmissibility ratio*. It quantifies how strongly disturbances couple into the rigid-body mode relative to how effectively the control input can actuate that mode. A larger disturbance channel $D_0$ or weaker control channel $B_0$ increases $\bar{\rho}_{00}$, indicating degraded disturbance-rejection capability, whereas stronger actuation along $B_0$ reduces this term, reflecting improved suppression of rigid-body perturbations. From a design perspective, $\bar{\rho}_{00}$ therefore provides a direct metric for actuator effectiveness in rigid-body disturbance rejection, complementing the stable-mode contribution:

$$\bar{\rho}_{ss} := \mathrm{tr}\big(\bar{W}_{ss}^{-1}\bar{\Sigma}_{ss}\big), \tag{59}$$

which is determined by the damping and modal properties of the asymptotically stable subsystem. Together, the two terms define the steady-state metric:

$$\bar{\rho} = \bar{\rho}_{ss} + \bar{\rho}_{00}, \tag{60}$$

cleanly separating the contributions of stable and rigid-body modes and enabling transparent trade-offs in control design.

Moreover, the availability of an explicit analytical expression eliminates the need for repeated numerical integration of the differential Lyapunov equations, thus significantly reducing the computational cost associated with performance evaluation and controller synthesis. The blockwise characterization also offers structural insights into how the system matrices $(A, B, D)$ influence the disturbance-rejection capability, which can be exploited in actuator placement and robust control system design.

To illustrate the practical implications of the proposed metric and to demonstrate how it overcomes the limitations of the standard DoDR formulation, we next present numerical examples. These examples highlight the accuracy, efficiency, and interpretability of the closed-form solution, while validating its consistency with time-domain simulations for systems involving both asymptotically stable modes and a single zero eigenvalue mode.

## 4. Numerical Examples on Disturbance-Rejection Controllability and Actuator Allocation

In this section, we investigate the disturbance-rejection controllability of a mass–spring–damper chain with a rigid-body mode, which provides a simple yet insightful testbed for actuator allocation problems. The system consists of $N$ identical masses connected in series by springs and dampers, without any springs or dampers attached to the ground. This configuration inherently yields a rigid-body translational mode in addition to the stable oscillatory modes. We consider an external disturbance acting on a specific mass and examine how the placement of a limited number of actuators affects the steady-state disturbance-rejection metric introduced in the previous sections. Two representative cases are studied: (i) $N = 2$: We demonstrate numerical efficiency and numerical stability advantages of the proposed algebraic steady-state computation over conventional finite-horizon integration. (ii) $N = 9$: Using the proposed steady-state metric, we investigate the actuator placement problem across all candidate sites and interpret the physical plausibility of the selected location.

### *4.1. System Description*

Consider $N$ masses connected in a one-dimensional chain by linear springs and dampers, as illustrated in Figure 1. Each mass is constrained to a single translational degree of freedom $y_i(t)$, so that the system has $N$ generalized coordinates. Each spring and damper connects two adjacent masses; thus, no stiffness or damping links to the ground are present, which introduces a rigid-body translational mode in addition to the oscillatory modes. Setting the mass, damping, and stiffness parameters to unity $(m = c = k = 1)$ for simplicity, the equations of motion for the system reduce to

$$\ddot{y}(t) + C\dot{y}(t) + Ky(t) = Fu(t) + Gw(t), \tag{61}$$

where

$$y(t) = [y_1(t), y_2(t), \ldots, y_N(t)]^\top \tag{62}$$

is the displacement vector, and the standard tridiagonal damping and stiffness matrices are identical:

$$K = C = \begin{bmatrix} 1 & -1 & & \\ -1 & 2 & -1 & \\ & \ddots & \ddots & \ddots \\ & & -1 & 1 \end{bmatrix}. \tag{63}$$

The external input $u(t)$ represents actuator forces, while $w(t)$ denotes disturbance inputs. Their distributions across the masses are defined by the matrices $F$ and $G$, respectively, which select the locations of actuators and disturbances as canonical basis vectors.

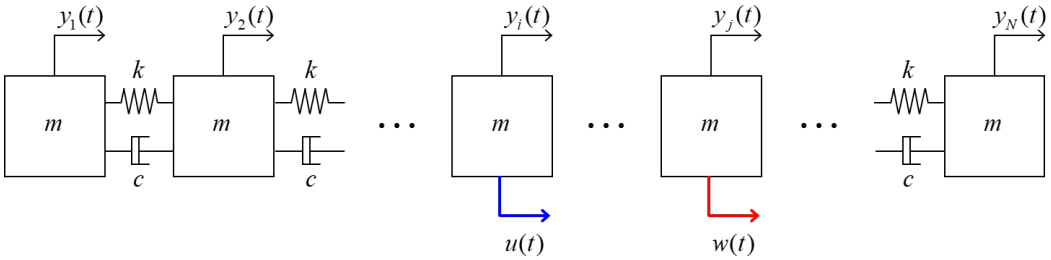


**Figure 1.** Mass–spring–damper chain considered in this study. The system consists of $N$ identical masses connected in series by springs and dampers, with no ground attachments. This configuration inherently produces a rigid-body mode in addition to the oscillatory modes. Actuator inputs $u(t)$ and disturbances $w(t)$ act at specific mass locations as indicated by the matrices $F$ and $G$.

Defining the state vector

$$z(t) = [y^\top(t), \dot{y}^\top(t)]^\top \in \mathbb{R}^{2N}, \tag{64}$$

the system (61) can be written in the state-space form

$$\dot{z}(t) = A_z z(t) + B_z u(t) + D_z w(t) \tag{65}$$

with

$$A_z = \begin{bmatrix} 0 & I_N \\ -K & -C \end{bmatrix}, \qquad B_z = \begin{bmatrix} 0 \\ F \end{bmatrix}, \qquad D_z = \begin{bmatrix} 0 \\ G \end{bmatrix}. \tag{66}$$

Because no springs or dampers connect the chain to a fixed point, the matrix $A_z$ always contains a pair of zero eigenvalues, corresponding to the rigid-body translational mode.

*4.2. Numerical Efficiency and Stability Comparison ($N = 2$)*

We consider the free–free two-mass chain with $(m, c, k) = (1, 1, 1)$ and the state vector $z(t) = [y^\top(t), \dot{y}^\top(t)]^\top \in \mathbb{R}^4$. In this case, the stiffness and damping matrices are identical and given by

$$K = C = \begin{bmatrix} 1 & -1 \\ -1 & 1 \end{bmatrix}. \tag{67}$$

We apply the block-orthonormal modal transform $T = \mathrm{blkdiag}(\Phi, \Phi)$ with the mass-orthonormal eigenmatrix

$$\Phi = \frac{1}{\sqrt{2}} \begin{bmatrix} -1 & -1 \\ 1 & -1 \end{bmatrix}, \qquad \Phi^\top \Phi = I_2, \qquad \Phi^\top K \Phi = \Phi^\top C \Phi = \mathrm{diag}(2, 0). \tag{68}$$

Defining the modal coordinates $\tilde{z} = T^{-1} z = [q^\top, \dot{q}^\top]^\top$ with $q = [q_1, q_2]^\top = \Phi^\top y$, the dynamics decouple into an oscillatory mode $(q_1, \dot{q}_1)$ and a rigid-body mode $(q_2, \dot{q}_2)$. In particular, $q_1$ corresponds to the relative displacement between the two masses, while $q_2$ represents their common translation.

Since $q_2$ corresponds to a pure translational motion that does not influence the internal dynamics, it is excluded from the state definition to maintain a single zero-eigenvalue mode associated with the rigid-body motion. Accordingly, the state vector is defined as

$$x(t) = [q_1(t), \dot{q}_1(t), \dot{q}_2(t)]^\top, \tag{69}$$

which represents the essential dynamic variables capturing both the oscillatory mode $(q_1, \dot{q}_1)$ and the rigid-body velocity $\dot{q}_2$. This formulation ensures that the system retains only one rigid-body degree of freedom, consistent with the single zero-eigenvalue assumption considered throughout this study. This reduction yields the block-diagonal form in (14):

$$A_s = \begin{bmatrix} 0 & 1 \\ -2 & -2 \end{bmatrix}, \qquad A_0 = 0 \in \mathbb{R}. \tag{70}$$

If we define the input matrices $B_i$ and the disturbance matrices $D_j$ as those corresponding to the force input at the $i$-th location and the disturbance at the $j$-th location, respectively, we obtain

$$B_1 = D_1 = \tfrac{1}{\sqrt{2}} \begin{bmatrix} 0 \\ -1 \\ -1 \end{bmatrix}, \qquad B_2 = D_2 = \tfrac{1}{\sqrt{2}} \begin{bmatrix} 0 \\ 1 \\ -1 \end{bmatrix}. \tag{71}$$

Partitioning into the stable and zero-eigenvalue blocks consistent with (12) and (13), we have

$$B_{1,s} = \tfrac{1}{\sqrt{2}} \begin{bmatrix} 0 \\ -1 \end{bmatrix}, \quad B_{1,0} = -\tfrac{1}{\sqrt{2}}, \qquad B_{2,s} = \tfrac{1}{\sqrt{2}} \begin{bmatrix} 0 \\ 1 \end{bmatrix}, \quad B_{2,0} = -\tfrac{1}{\sqrt{2}}. \tag{72}$$

Following these matrices, we evaluate the disturbance-rejection controllability using two approaches. First, the *conventional finite-horizon DoDR* is computed by integrating the differential Lyapunov equations in (7)–(8) and then applying (4); the matrix ODEs are integrated with a classical fourth-order Runge–Kutta (RK4) scheme. Second, the *proposed steady-state DoDR* is obtained directly from the closed-form expression in Theorem 1 (see (55)). The results are shown in Figure 2. For the input–disturbance pairs $(B_1, D_1)$ and $(B_2, D_2)$, the controllability and disturbance Gramians are identical, and thus, the finite-horizon DoDR coincides with the steady-state value immediately. For the remaining cases, the finite-horizon DoDR trajectories gradually converge to the steady-state values predicted

by our formula as the horizon increases, confirming that the proposed expression exactly captures the steady-state limit of the conventional DoDR.

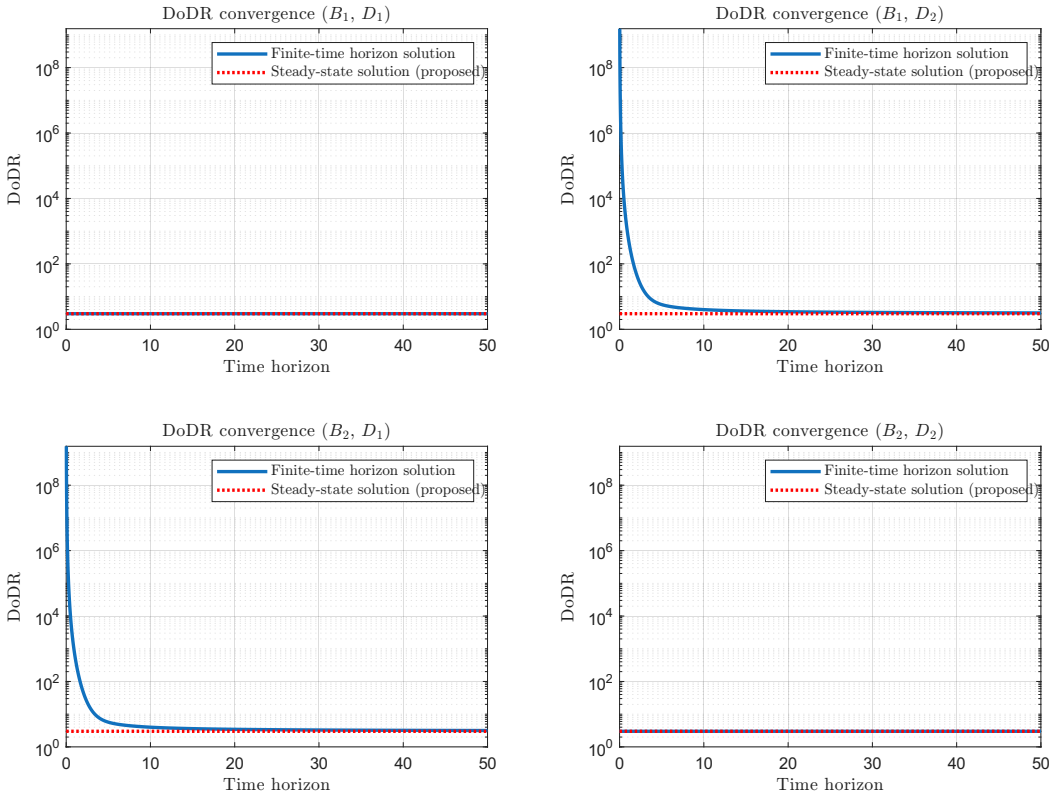


**Figure 2.** Finite-horizon DoDR (solid lines) versus steady-state DoDR (red dashed lines) for the two-mass chain ($N = 2$). Results are shown for all input–disturbance pairs $(B_1, D_1)$, $(B_2, D_1)$, $(B_1, D_2)$, and $(B_2, D_2)$. The finite-horizon trajectories converge to the steady-state values, confirming the validity of the proposed formulation.

The numerical advantages of the proposed expression are illustrated in Figure 3. At the beginning of the integration, i.e., for small horizon times, the condition numbers are inevitably large due to transient effects. In cases where the solution truly converges, one would expect the condition numbers to eventually settle to bounded values. However, as seen in the figure, beyond a certain horizon the condition numbers instead grow linearly with time, reflecting the divergence induced by the rigid-body mode. Because the rigid-body mode induces linear growth of the zero-block Gramians, the condition numbers of both $W(t)$ and $\Sigma(t)$ deteriorate with time. This ill-conditioning can severely affect the computation of $W^{-1}(t)$ required by the finite-horizon Formula (4). In contrast, the proposed steady-state DoDR is obtained from purely algebraic closed forms that remain well-conditioned, yielding the exact steady-state value $\bar{\rho}$ without inverting poorly conditioned time-varying Gramians. Hence, for systems with a rigid-body mode, the steady-state formulation is advantageous both in *accuracy* (exact asymptotic value) and *numerical robustness* (no large-$t$ ill-conditioning).

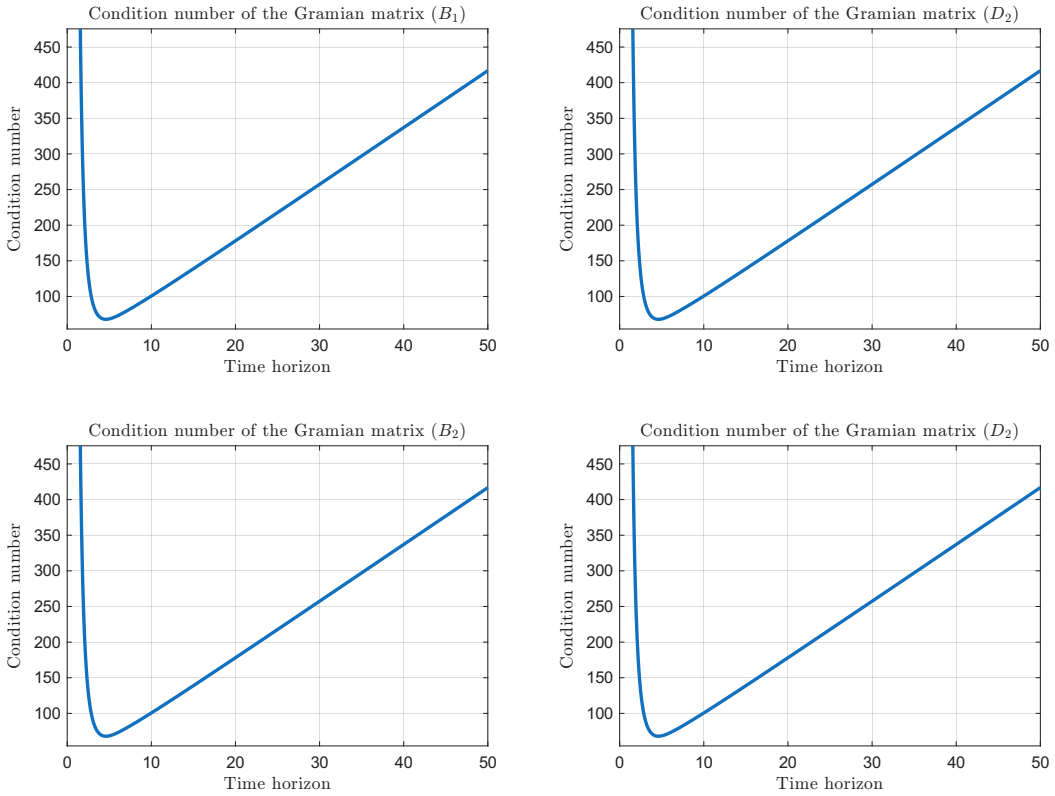


**Figure 3.** Condition numbers of the controllability Gramian $W(t)$ and disturbance Gramian $\Sigma(t)$ in the two-mass chain ($N = 2$). Both condition numbers grow linearly with time due to the rigid-body mode, while the proposed steady-state formulation avoids such ill-conditioning.

### *4.3. Actuator Placement and Interpretation of Results ($N = 9$)*

In this subsection, we extend the analysis to a nine-mass chain to examine actuator placement under more complex modal interactions. Having already confirmed in the two-mass case that the proposed steady-state formulation provides both numerical accuracy and robustness, we now demonstrate that the method can be applied without difficulty to higher-dimensional systems. Specifically, we consider nine distinct disturbance scenarios, each corresponding to a unit disturbance applied to one of the masses. For each disturbance case, the proposed steady-state disturbance-rejection metric is evaluated across all nine candidate actuator locations, yielding a total of $9 \times 9 = 81$ combinations. This comprehensive set of results enables us to systematically compare the effectiveness of different actuator placements. Based on the computed metrics, we identify locations that provide superior disturbance-rejection controllability as well as those that lead to poor performance, and we interpret these findings in relation to the underlying structural dynamics of the chain system.

The computed values of the proposed metric for all 81 input–disturbance combinations are summarized in Figure 4. In this figure, the horizontal axis corresponds to the actuator index, indicating the mass location $i$ where the input matrix $B_i$ is applied. The vertical axis represents the disturbance index, indicating the mass location $i$ where the disturbance matrix $D_i$ acts. The metric values are visualized using a colormap, with the accompanying color bar indicating the magnitude of the steady-state disturbance-rejection metric. This representation allows for a direct comparison of actuator effectiveness across all candidate placements under different disturbance scenarios.

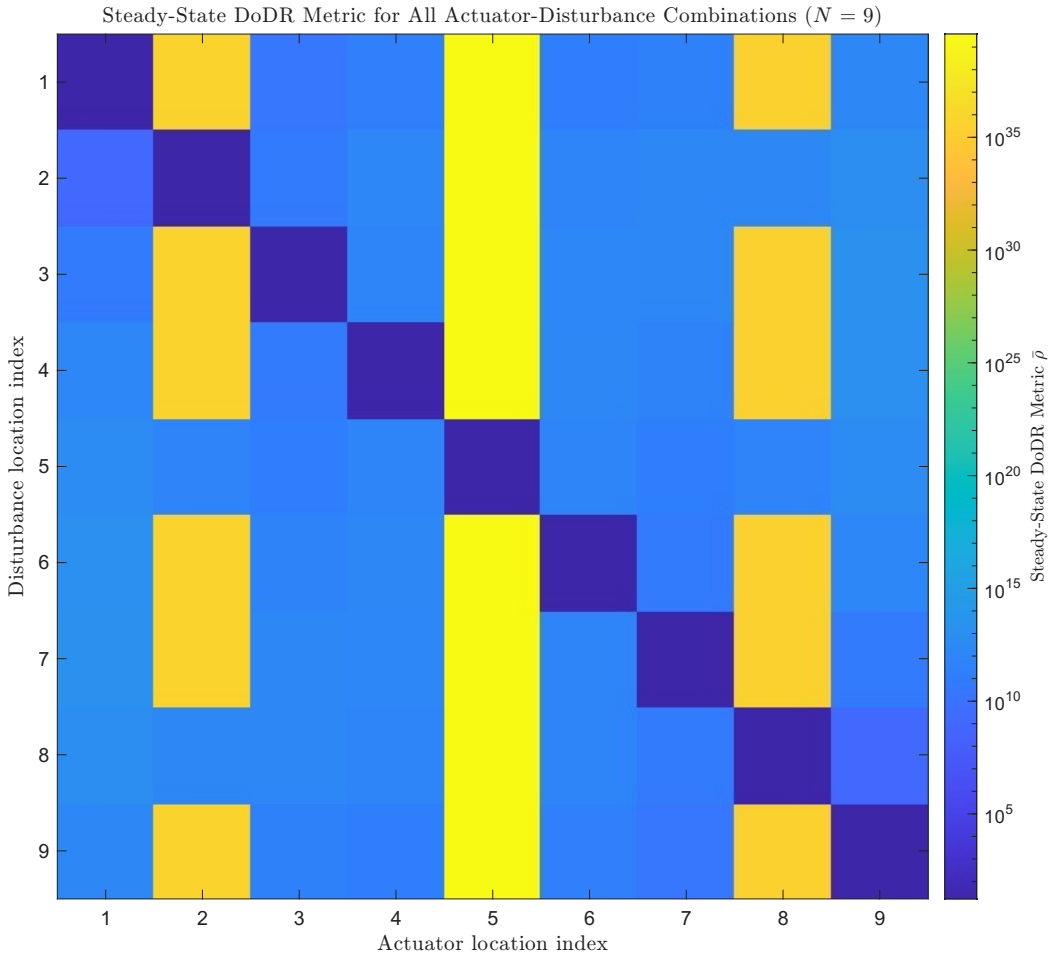


**Figure 4.** Steady-state DoDR metric values for the nine-mass chain ($N = 9$) across all 81 actuator–disturbance combinations. The colormap shows that matched actuator–disturbance pairs yield the lowest metric values, while nodal locations of dominant modes result in poor performance.

The most immediate observation from Figure 4 is that the smallest metric values are obtained in the *matched disturbance cases*, where the actuator is placed at the same location as the disturbance. Since the DoDR metric is defined as the minimal control energy required for disturbance rejection, this behavior clearly indicates that matched placement provides the most favorable configuration for disturbance suppression. This trend is also consistent with results reported in the literature on finite-horizon DoDR formulations [24]. Hence, the steady-state DoDR confirms the physically intuitive conclusion that the optimal actuator location is exactly the disturbance location.

Across almost all disturbance scenarios, the least effective actuator position is the 5th mass. This is because the 5th position coincides with the nodal point of the first oscillatory mode (excluding the rigid-body mode). When the actuator is placed at this location, the dominant first mode cannot be effectively controlled, making disturbance rejection particularly difficult. However, when the disturbance itself acts on the 5th mass, the matched condition again yields a small metric value. This can be explained by the fact that no significant excitation of the first mode occurs when the disturbance is applied at its nodal point.

In addition to the 5th mass, actuator placements at the 2nd and 8th masses also yield relatively large metric values. These positions are near the nodal points of the second mode, which is the next dominant oscillatory mode of the chain. This explains why the disturbance suppression capability is reduced when actuators are placed at these locations. A notable feature, however, is observed when the disturbance is applied at these nodal

positions (i.e., at masses 2, 5, or 8). In such cases, actuator placements at other nodal positions may still result in comparatively small metric values. For example, when the disturbance acts at the 2nd mass, placing the actuator at the 8th mass yields a lower metric than expected. This occurs because both positions are ineffective in exciting the second mode, so the disturbance itself excites little of the mode that would otherwise be difficult to control. A similar interpretation applies to the cases where disturbances act at the 5th or 8th masses.

To verify the validity of the DoDR-based actuator placement results presented in Figure 4, additional simulations were conducted to evaluate the actual control performance under disturbance conditions. The disturbance was applied at the 9th mass location ($D_9$), and three actuator configurations were considered: actuators placed at the 5th, 8th, and 9th mass positions ($B_5$, $B_8$, and $B_9$), respectively. As shown in Figure 4, the DoDR metric predicts that the optimal actuator location is $B_9$, while $B_5$ corresponds to the lowest disturbance-rejection capability. To examine whether these predictions are consistent with closed-loop performance, a linear quadratic regulator (LQR) controller was implemented for each configuration. The weighting matrices of the LQR were adjusted such that the overall input energy remained comparable across cases, allowing a fair comparison of control effectiveness. Figure 5 illustrates the time histories of the state power $\|x(t)\|^2$ and input power $\|u(t)\|^2$. The results clearly show that the actuator at $B_9$ achieves the lowest state power and hence the strongest disturbance suppression, followed by $B_8$ and $B_5$, in agreement with the DoDR predictions. These results confirm that the proposed DoDR metric consistently reflects the system's actual disturbance-rejection performance observed in time-domain control simulations.

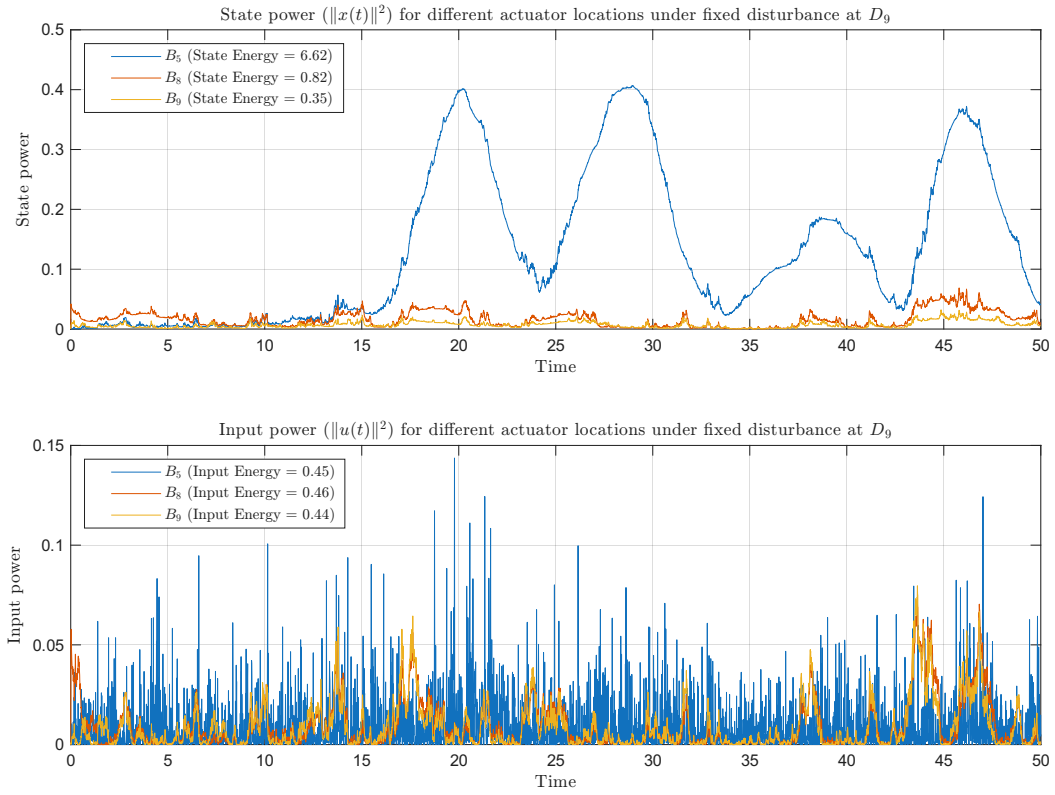


**Figure 5.** Verification of the proposed DoDR metric through LQR control simulations. A disturbance was applied to the 9th mass, and responses were compared for actuator placements at $B_5$, $B_8$, and $B_9$. The actuator located at $B_9$, which corresponds to the smallest DoDR value, exhibited the best disturbance-rejection performance.

All these results are physically consistent and provide clear evidence that the proposed steady-state DoDR not only guarantees numerical robustness in the presence of rigid-body modes but also yields actuator placement outcomes that are physically meaningful. This demonstrates the practical utility of the proposed formulation in guiding actuator placement decisions for systems that include rigid-body dynamics.

## 5. Conclusions and Future Works

This study presented a steady-state formulation of the disturbance-rejection controllability (DoDR) metric for LTI systems with both asymptotically stable modes and a rigid-body mode. By exploiting a blockwise decomposition of the system dynamics, we established the asymptotic behavior of the controllability and disturbance Gramians and derived a closed-form steady-state solution. The resulting expression separates the contributions of the stable subsystem and the rigid-body mode, yielding a finite and computationally efficient performance index even when the conventional DoDR becomes ill-posed. This closed-form characterization also provides a clear physical interpretation: the rigid-body contribution appears as a disturbance-to-control transmissibility ratio, while the stable-mode contribution reflects the modal damping properties.

Numerical examples with mass–spring–damper chains demonstrated both the accuracy and physical validity of the proposed metric. In the two-mass case, the steady-state formulation reproduced the exact limit of the finite-horizon DoDR while avoiding numerical ill-conditioning. In the nine-mass case, actuator placement analysis revealed results consistent with modal structures, such as identifying nodal positions as unfavorable actuator sites. The proposed steady-state DoDR formulation was further validated through simulation, where the quantitatively evaluated disturbance-rejection capability showed consistent trends with the predicted DoDR values. This confirms that the DoDR metric enables a reliable quantitative assessment of disturbance suppression performance based solely on system characteristics. These findings confirm that the proposed steady-state DoDR not only ensures numerical robustness but also offers meaningful guidance for actuator placement in systems involving rigid-body dynamics.

The present work focused on systems with a single zero eigenvalue mode. A natural extension is to generalize the analysis to systems with multiple rigid-body modes, which frequently arise in flexible multibody dynamics and aerospace structures. In such cases, the zero-eigenvalue subspace becomes multidimensional, and the corresponding sub-blocks of the controllability and disturbance Gramians exhibit coupled growth patterns rather than the scalar behavior analyzed here. Extending the steady-state DoDR formulation to this setting requires treating the $(A_0, B_0, D_0)$ submatrices as multi-dimensional zero-mode blocks and analyzing the asymptotic behavior of their Schur complements. Although the closed-form expressions derived in this paper no longer hold directly, the same blockwise decomposition principle can be applied to derive generalized DoDR metrics for systems with multiple zero eigenvalues. Building upon the framework developed here, future research will address these blockwise behaviors and derive corresponding steady-state expressions for the DoDR metric, thereby broadening the applicability of the proposed approach.

**Author Contributions:** Conceptualization, H.L.; methodology, H.L.; validation, J.P.; formal analysis, H.L. and J.P.; investigation, H.L. and J.P.; writing—original draft preparation, H.L.; writing—review and editing, J.P.; supervision, J.P.; project administration, H.L.; funding acquisition, J.P. All authors have read and agreed to the published version of the manuscript.

**Funding:** This work was supported by the research grant of Kongju National University Industry-University Cooperation Foundation in 2025, and by Chungnam National University.

**Institutional Review Board Statement:** Not applicable.

**Informed Consent Statement:** Not applicable.

**Data Availability Statement:** The original contributions presented in this study are included in this article.

**Conflicts of Interest:** The authors declare no conflicts of interest.

## References


1. Paige, C. Properties of numerical algorithms related to computing controllability. *IEEE Trans. Autom. Control* **1981**, *26*, 130–138. [CrossRef]
2. Hughes, P.; Skelton, R. Controllability and observability of linear matrix-second-order systems. *J. Appl. Mech.* **1980**, *47*, 415–420. [CrossRef]
3. Hamdan, A.; Nayfeh, A. Measures of modal controllability and observability for first-and second-order linear systems. *J. Guid. Control Dyn.* **1989**, *12*, 421–428. [CrossRef]
4. Tarokh, M. Measures for controllability, observability and fixed modes. *IEEE Trans. Autom. Control* **1992**, *37*, 1268–1273. [CrossRef]
5. Viswanathan, C.; Longman, R.; Likins, P. A degree of controllability definition-fundamental concepts and application to modal systems. *J. Guid. Control Dyn.* **1984**, *7*, 222–230. [CrossRef]
6. Müller, P.; Weber, H. Analysis and optimization of certain qualities of controllability and observability for linear dynamical systems. *Automatica* **1972**, *8*, 237–246. [CrossRef]
7. Marx, B.; Koenig, D.; Georges, D. Optimal sensor/actuator location for descriptor systems using Lyapunov-like equations. In Proceedings of the 41st IEEE Conference on Decision and Control, Las Vegas, NV, USA, 10–13 December 2002; Volume 4, pp. 4541–4542.
8. Marx, B.; Koenig, D.; Georges, D. Optimal sensor and actuator location for descriptor systems using generalized gramians and balanced realizations. In Proceedings of the 2004 American Control Conference, Boston, MA, USA, 30 June–2 July 2004; Volume 3, pp. 2729–2734.
9. Singh, A.K.; Hahn, J. Determining optimal sensor locations for state and parameter estimation for stable nonlinear systems. *Ind. Eng. Chem. Res.* **2005**, *44*, 5645–5659. [CrossRef]
10. Singh, A.K.; Hahn, J. Sensor location for stable nonlinear dynamic systems: Multiple sensor case. *Ind. Eng. Chem. Res.* **2006**, *45*, 3615–3623. [CrossRef]
11. Shaker, H.R.; Stoustrup, J. An interaction measure for control configuration selection for multivariable bilinear systems. *Nonlinear Dyn.* **2013**, *72*, 165–174. [CrossRef]
12. Tahavori, M. Model reduction via truncated cross-gramian for bilinear systems. In Proceedings of the 2021 International Conference on Recent Advances in Mathematics and Informatics (ICRAMI), Tebessa, Algeria, 21–22 September 2021; pp. 1–5.
13. Zhao, S.; Pasqualetti, F. Networks with diagonal controllability Gramian: Analysis, graphical conditions, and design algorithms. *Automatica* **2019**, *102*, 10–18. [CrossRef]
14. Babazadeh, M. Gramian-based vulnerability analysis of dynamic networks. *IET Control Theory Appl.* **2022**, *16*, 625–637. [CrossRef]
15. Hać, A.; Liu, L. Sensor and actuator location in motion control of flexible structures. *J. Sound Vib.* **1993**, *167*, 239–261. [CrossRef]
16. Roh, H.S.; Park, Y. Actuator and exciter placement for flexible structures. *J. Guid. Control Dyn.* **1997**, *20*, 850–856. [CrossRef]
17. Shaker, H.R.; Tahavori, M. Optimal sensor and actuator location for unstable systems. *J. Vib. Control* **2013**, *19*, 1915–1920. [CrossRef]
18. Seyed Sakha, M.; Shaker, H.R.; Tahavori, M. Optimal sensors and actuators placement for large-scale switched systems. *Int. J. Dyn. Control* **2019**, *7*, 147–156. [CrossRef]
19. Satheesh, T.; Aravinth, N.; Sakthivel, R.; Kwon, O.M. Improved intermediate estimator-based security control for networked periodic piecewise stochastic systems with attacks and additive delays. *Chaos Solitons Fractals* **2025**, *198*, 116476. [CrossRef]
20. Satheesh, T.; Kayalvizhi, M.; Sakthivel, R.; Sozhaeswari, P. Finite-Time Secured Non-Fragile Control Design for Engine Throttle Valve System with Multiple Attacks Under Proportional Integral Observer. *Int. J. Robust Nonlinear Control* **2025**, *35*, 4201–4211. [CrossRef]
21. Hovd, M.; Skogestad, S. Simple frequency-dependent tools for control system analysis, structure selection and design. *Automatica* **1992**, *28*, 989–996. [CrossRef]
22. Cao, Y.; Rossiter, D.; Owens, D. Input selection for disturbance rejection under manipulated variable constraints. *Comput. Chem. Eng.* **1997**, *21*, S403–S408. [CrossRef]
23. Mirza, M.A.; Van Niekerk, J.L. Optimal actuator placement for active vibration control with known disturbances. *J. Vib. Control* **1999**, *5*, 709–724. [CrossRef]
24. Kang, O.; Park, Y.; Park, Y.; Suh, M. New measure representing degree of controllability for disturbance rejection. *J. Guid. Control Dyn.* **2009**, *32*, 1658–1661. [CrossRef]

25. Lee, H.; Park, Y. Degree of disturbance rejection capability for linear anti-stable systems. In Proceedings of the 2014 14th International Conference on Control, Automation and Systems (ICCAS 2014), Seoul, Republic of Korea, 22–25 October 2014; pp. 154–156.
26. Lee, H.; Park, Y. Degree of disturbance rejection capability for linear marginally stable systems. In Proceedings of the 2015 15th International Conference on Control, Automation and Systems (ICCAS), Busan, Republic of Korea, 13–16 October 2015; pp. 307–310.
27. Xia, Y.; Yin, M.; Cai, C.; Zhang, B.; Zou, Y. A new measure of the degree of controllability for linear system with external disturbance and its application to wind turbines. *J. Vib. Control* **2018**, *24*, 739–759. [CrossRef]
28. Xia, Y.; Yin, M.; Li, R.; Liu, D.; Zou, Y. Integrated structure and maximum power point tracking control design for wind turbines based on degree of controllability. *J. Vib. Control* **2019**, *25*, 397–407. [CrossRef]
29. Xia, Y.; Li, R.; Yin, M.; Zou, Y. A quantitative measure of the degree of output controllability for output regulation control systems: Concept, approach, and applications. *J. Vib. Control* **2022**, *28*, 2803–2815. [CrossRef]
30. Jeong, I.; Park, Y. Input energy minimization with acoustic potential energy constraint for active noise control system. *J. Vib. Control* **2025**, *31*, 444–456. [CrossRef]
31. Zhou, K.; Salomon, G.; Wu, E. Balanced realization and model reduction for unstable systems. *Int. J. Robust Nonlinear Control. IFAC-Affil. J.* **1999**, *9*, 183–198. [CrossRef]
32. Lee, H.; Park, Y. Degree of controllability for linear unstable systems. *J. Vib. Control* **2016**, *22*, 1928–1934. [CrossRef]
33. Lee, H.; Park, J. Quantitative controllability metric for disturbance rejection in linear unstable systems. *Mathematics* **2024**, *13*, 6. [CrossRef]
34. Alves da Silveira, O.A.; Ono Fonseca, J.S.; Santos, I.F. Actuator topology design using the controllability Gramian. *Struct. Multidiscip. Optim.* **2015**, *51*, 145–157. [CrossRef]
35. Halevi, Y. Approximated gramians and balanced realization of lightly damped flexible structures. *IEEE Trans. Autom. Control* **2002**, *47*, 193–198. [CrossRef]
36. Brand, Z.; Cole, M.O.T. Mini-max optimization of actuator/sensor placement for flexural vibration control of a rotating thin-walled cylinder over a range of speeds. *J. Sound Vib.* **2021**, *506*, 116105. [CrossRef]
37. Brand, Z.; Cole, M.O.T. Controllability and actuator placement optimization for active damping of a thin rotating ring with piezo-patch transducers. *J. Sound Vib.* **2020**, *472*, 115172. [CrossRef]
38. Lee, H. Controllability measure for disturbance rejection capabilities of control systems with undamped flexible structures. *J. Frankl. Inst.* **2024**, *361*, 107320. [CrossRef]
39. Chen, B.M.; Lin, Z.; Shamash, Y. *Linear Systems Theory: A Structural Decomposition Approach*; Springer Science & Business Media: Berlin/Heidelberg, Germany, 2004.
40. Horn, R.A.; Johnson, C.R. *Matrix Analysis*; Cambridge University Press: Cambridge, UK, 2012.


**Disclaimer/Publisher's Note:** The statements, opinions and data contained in all publications are solely those of the individual author(s) and contributor(s) and not of MDPI and/or the editor(s). MDPI and/or the editor(s) disclaim responsibility for any injury to people or property resulting from any ideas, methods, instructions or products referred to in the content.